

# Bidirectional Generative Pre-training for Improving Time Series Representation Learning

Ziyang Song<sup>1</sup> Qincheng Lu<sup>1</sup> He Zhu<sup>1</sup> Yue Li<sup>1</sup>

## Abstract

Learning time-series representations for discriminative tasks has been a long-standing challenge. Current pre-training methods are limited in either unidirectional next-token prediction or randomly masked token prediction. We propose a novel architecture called **Bidirectional Timely Generative Pre-trained Transformer (BiTimelyGPT)**, which pre-trains on time-series data by both next-token and previous-token predictions in alternating transformer layers. This pre-training task preserves original distribution and data shapes of the time-series. Additionally, the full-rank forward and backward attention matrices exhibit more expressive representation capabilities. Using biosignal data, BiTimelyGPT demonstrates superior performance in predicting neurological functionality, disease diagnosis, and physiological signs. By visualizing the attention heatmap, we observe that the pre-trained BiTimelyGPT can identify discriminative segments from time-series sequences, even more so after fine-tuning on the task.

## 1. Introduction

Time-series data can provide valuable insights into patient health status and their clinical outcomes (Ma et al., 2023; Edele et al., 2021). One useful application is to learn temporal representations and use them to achieve accurate sequence-to-vector (seq2vec) prediction tasks. In particular, biosignals such as electroencephalogram and electrocardiogram are extensively utilized for diverse applications such as disease diagnosis (Phan et al., 2021), neurophysiological functionality (Stirling et al., 2020), and vital signal estimation (Reiss et al., 2019b). A long-standing challenge lies in learning meaningful representations from the time-series, particularly in scenarios with limited labeled data. To address this problem, self-supervised learning designs pre-training

<sup>1</sup>School of Computer Science, McGill University, Montreal, Canada. Correspondence to: Yue Li <yueli@cs.mcgill.ca>.

Preliminary work. Under review by the International Conference on Machine Learning (ICML). Do not distribute.

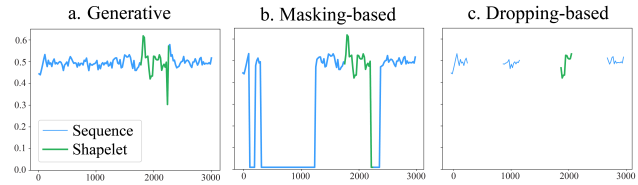


Figure 1. Three pre-training methods on a normalized time-series with a shapelet learned by pyts package (Faouzi & Janati, 2020). **a. Generative** pre-training maintains the original distribution and time-series shapelet. **b. Masking-based** pre-training masks segments to zeros, resulting in distribution shift. **c. Dropping-based** pre-training randomly discards segments up to 70% of the data and thus disrupts the discriminative shapelet.

tasks to learn representations from unlabeled time-series data, thereby improving performance in downstream tasks (Ma et al., 2023).

Recent advancements in Transformer pre-trained models (PTMs) for Natural Language Processing and Computer Vision have led to their exploration in time-series representation learning. Self-supervised learning methods in this domain fall primarily into two categories: masking-based and dropping-based pre-training. Masking-based methods, such as PatchTST, randomly mask segments of time-series to zeros and then reconstruct them using learned representations (Zerveas et al., 2021; Nie et al., 2023). However, as shown in Figure 1.b, these methods suffer from data distribution shift, which introduce noises into the pre-training stage and degrade the quality of the learned representations. Unlike images and text data (Devlin et al., 2019; Dosovitskiy et al., 2021), distribution shift presents a larger challenge for time-series, where the introduced zeros are substantially deviate from the actual signals (Zhang et al., 2023). In contrast, Cross-Reconstruction Transformer (CRT) adopts a dropping-based method to circumvent distribution shift by discarding and reconstructing data segments (Zhang et al., 2023). However, as shown in Figure 1.c, this method risk disrupting shapelets, which are discriminative subsequences of time-series data crucial for identifying the target class labels of the sequence (Ye & Keogh, 2009; Grabocka et al., 2014). As a potential solution, GPT adopts a next-token prediction task, which effectively preserves both the original distribution and time-series shapelets without changing the

data (Figure 1.a). Despite GPT’s efficacy in representation learning in diverse domains, its potential in time-series domain is still underexplored (Radford & Narasimhan, 2018).

While GPT is exceptionally effective for generative forecasting tasks using past contexts, its causal attention (Figure 2.b) is less effective in discriminative tasks that require bidirectional contexts (Devlin et al., 2019). Using bidirectional self-attention (Figure 2.a), PatchTST and CRT achieve superior performance in these tasks. While this self-attention mechanism captures bidirectional contexts, its attention matrix is low rank and thus faces a loss of expressiveness (Bhojanapalli et al., 2020). These limitations underscore the necessity for an architecture that extracts bidirectional contexts with an expressive, full-rank attention matrix.

In this study, we aim to improve time-series representation learning via a novel pre-training strategy towards improving downstream seq2vec prediction tasks. To this end, we propose the **Bidirectional Timely Generative Pre-trained Transformer (BiTimelyGPT)** that integrates bidirectionality into generative pre-training to improve time-series representation learning. It introduces a Next-Previous-Token Prediction pre-training task, preserving the original distribution and time-series shapelets without any data alterations. Our BiTimelyGPT model alternates forward and backward attention across layers, pre-training deep bidirectional representations through layers. Furthermore, both the forward and backward attention matrices in BiTimelyGPT are full-rank and thus exhibit expressive representation power (Bhojanapalli et al., 2020). The qualitative and quantitative results demonstrate the strengths of BiTimelyGPT over existing studies (Table 1), including data preservation, bidirectionality, and full-rankedness. This makes BiTimelyGPT a highly effective architecture for downstream discriminative tasks.

The key contributions of our research are threefold:

1. a Next-Previous-Token Prediction pre-training task preserves the original data distribution and time-series shapelets (Figure 1);
2. a **Bidirectionally Alternating AutoRegressive Modeling (BAAR)** framework alternately models left-to-right and right-to-left information, learning deep bidirectional contexts for discriminative tasks (Figure 2);
3. the full-rank forward and backward attention matrices exhibit expressive representation power (Figure 2).

## 2. Background

### 2.1. Transformer Architecture

Transformer is an encoder-decoder model architecture stacked by  $L$  layers of Transformer blocks (Vaswani et al.,

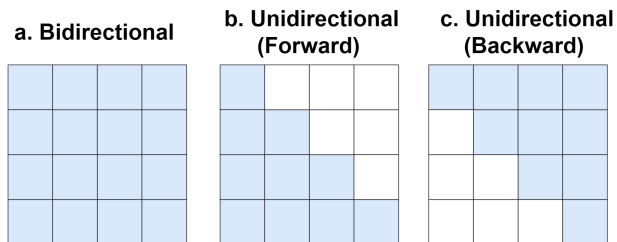


Figure 2. Bidirectional and unidirectional (forward and backward) attention matrices. Unlike bidirectional self-attention (a), BiTimelyGPT alternates forward (b) and backward (c) attention across layers, achieving bidirectionality and full-rankedness.

2017). Each block consists of a multi-head self-attention layer followed by a feed-forward layer. Given an input embedding  $\mathbf{X} \in \mathbb{R}^{N \times d}$ , where  $N$  is the number of tokens and  $d$  is the hidden dimension, the output of a self-attention layer is computed as follows.

$$\text{Attention}(\mathbf{X}) = \text{Softmax} \left( \underbrace{\frac{\mathbf{Q}\mathbf{K}^\top}{\sqrt{d}}}_{\overleftarrow{\mathbf{A}}} \right) \mathbf{V} \quad (1)$$

where  $\mathbf{Q}, \mathbf{K}, \mathbf{V} = \mathbf{X}\mathbf{W}_Q, \mathbf{X}\mathbf{W}_K, \mathbf{X}\mathbf{W}_V \in \mathbb{R}^{N \times d}$  are Query, Key, and Value matrices, respectively. The bidirectional attention matrix  $\overleftarrow{\mathbf{A}}$  captures the context of each token based on all other tokens in the sequence.

Among various transformers, GPT and BERT stand out as decoder-only and encoder-only architectures, respectively (Radford et al., 2019; Devlin et al., 2019). The causal Transformer GPT utilizes a masked self-attention mechanism:

$$\text{CausalAttention}(\mathbf{X}) = \text{Softmax} \left( \underbrace{\frac{\mathbf{Q}\mathbf{K}^\top}{\sqrt{d}} \odot \mathbf{C}}_{\overleftarrow{\mathbf{A}}} \right) \mathbf{V} \quad (2)$$

where both the mask matrix  $\mathbf{C}$  and forward attention matrix  $\overleftarrow{\mathbf{A}}$  are lower triangular. GPT’s Next-Token Prediction task effectively captures complex dependencies of natural language and thus excels in generative tasks. In contrast, BERT uses masking-based pre-training for deep bidirectional representations, which are crucial for discriminative tasks. Unlike BERT’s bidirectional attention in each layer, BiTimelyGPT alternates between forward and backward attention across layers, pre-training deep bidirectional representations through a generative task.

### 2.2. Bidirectional Recurrent Representation Learning

Deep Bidirectional LSTM (BiLSTM) trains forward and backward LSTMs independently at each layer, followed by concatenating the hidden states from both directions post-layer. Embeddings from Language Models (ELMo) also trains forward and backward LSTMs independently, but

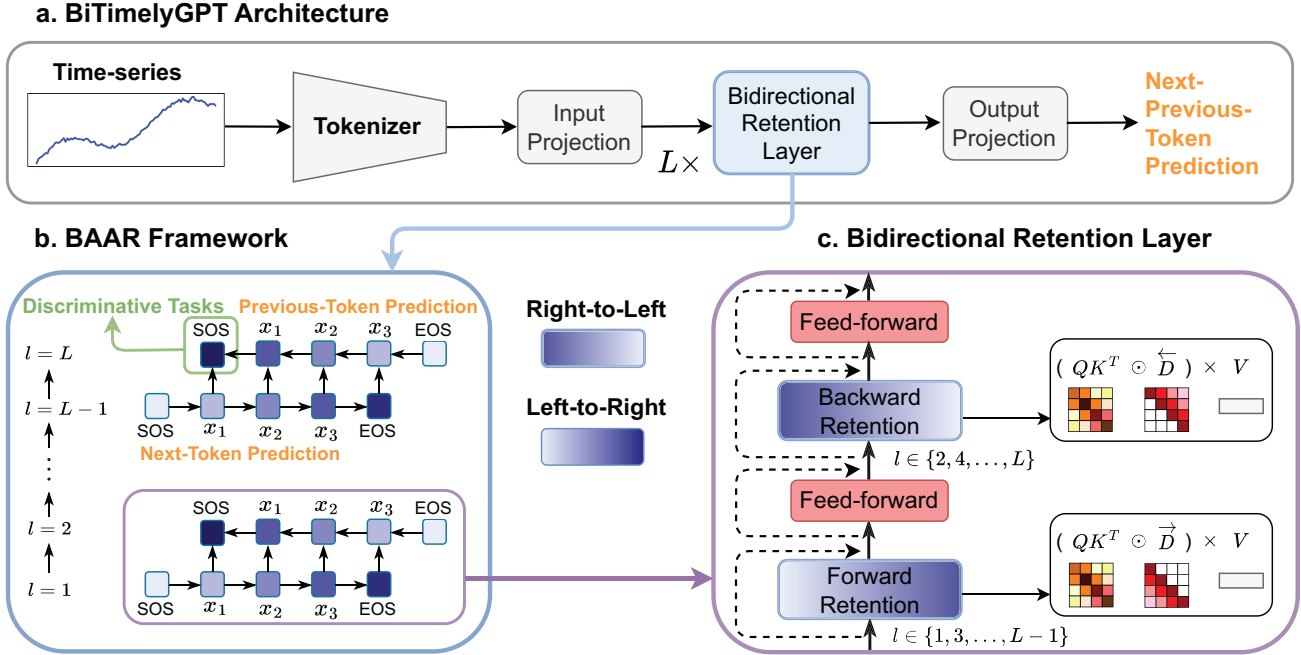


Figure 3. BiTimelyGPT overview. **a. BiTimelyGPT architecture** is stacked by a series of bidirectional retention layers, with an overflow of pre-training in Appendix A.2. **b. BAAR framework** (Section 3.1) alternately models left-to-right and right-to-left information across layers. It performs Next-Previous-Token Prediction on the final two layers and utilizes the [SOS] token in the final layer for discriminative tasks. **c. Bidirectional Retention Layer** (Section 3.2) alternates between the forward and backward retention mechanism across layers.

concatenates their outputs only in the final layer (Peters et al., 2018). Although ELMo effectively generates pre-trained contextualized representations for downstream tasks, its bidirectional context is not deep due to the shallow concatenation of left and right contexts (Devlin et al., 2019). In contrast, our proposed BAAR framework alternately models information from both directions across layers, allowing for *deep* bidirectional representation learning.

### 2.3. Recurrent Transformer RetNet

Extrapolatable position embedding (xPos) encodes relative position information into Query  $\hat{Q}_n$  and Key  $\hat{K}_m$  based on the distances between tokens  $n$  and  $m$  (Sun et al., 2023b):

$$\tilde{Q}_n \tilde{K}_m^\top = X_n W_Q (\gamma e^{i\theta})^{n-m} (X_m W_K)^\top = \hat{Q}_n \gamma^{n-m} \hat{K}_m^\top$$

with  $\hat{Q}_n = X_n W_Q e^{i\theta n}$ ,  $\hat{K}_m = X_m W_K e^{-i\theta m}$  (3)

where  $\theta$  and  $\gamma$  are rotation and exponential decay hyperparameters. The RetNet model introduces a retention mechanism based on the xPos embedding: (Sun et al., 2023a):

$$\vec{\text{Ret}}(X) = \underbrace{(\hat{Q} \hat{K}^\top \odot \vec{D})}_{\vec{R}} V, \quad \vec{D}_{nm} = \begin{cases} \gamma^{n-m}, & n \geq m \\ 0, & n < m \end{cases} \quad (4)$$

where  $\vec{D} \in \mathbb{R}^{N \times N}$  is a lower triangular decay matrix. The retention can be reformulated as an RNN for  $n$ -th timestep:

$$\vec{\text{Ret}}(X_n) = \hat{Q}_n S_n, \quad S_n = \hat{K}_n^\top V_n + \gamma S_{n-1} \quad (5)$$

TimelyGPT, built upon RetNet, offers two main advantages in ultra-long-term forecasting (Song et al., 2023). Firstly, TimelyGPT leverages xPos to encode trend and periodic temporal patterns into time-series representations. Moreover, its retention mechanism, reformulating itself as an RNN, inherently captures temporal dependencies. However, unidirectional TimelyGPT falls short in discriminative tasks compared to bidirectional CRT without convolution modules. To bridge this gap, we propose BiTimelyGPT, which leverages a novel BAAR framework, to integrate bidirectionality into autoregressive time-series modeling.

## 3. BiTimelyGPT Methodology

An input sequence of time-series  $x$  is denoted as  $\{x_1, x_2, \dots, x_T\}$  over  $T$  timesteps, with  $x_t$  comprising  $V$  features. As depicted in Figure 3.a, BiTimelyGPT utilizes a convolution-subsampling tokenizer with two 1-D convolution layers (Gulati et al., 2020), reducing the  $T \times V$  down to an  $N \times V$  sequence with  $N < T$ . These tokens are projected onto an input embedding  $X \in \mathbb{R}^{N \times d}$ , which is prepended and appended with [SOS] and [EOS] tokens (Radford

et al., 2021), respectively. Appendix A.2 depicts the details. As stated above, the goal of time-series representation learning in this study is to pre-train temporal representations for fine-tuning seq2vec tasks. Here, the output vector  $\hat{y}$  can be either a continuous variable for regression or a categorical variable for classification. We describe the BAAR framework in Section 3.1, the BiTimelyGPT pre-training in Section 3.2, and the desired full-ranked attention matrix as a result in Section 3.3. The notations of variables are defined in Appendix A.1.

### 3.1. Bidirectional Alternating Autoregressive Modeling

The BAAR framework presents a general approach for incorporating bidirectionality into autoregressive models. It alternates between left-to-right and right-to-left information flows depending on the odd and even layer indices, respectively. In the odd-indexed layers  $l \in \{1, 3, \dots, L-1\}$ , the forward model computes the probability of the sequence  $x$  by modeling the conditional probability of  $x_t$  given the history context  $(x_1, \dots, x_{t-1})$  (Bengio et al., 2000):

$$p(x_1, x_2, \dots, x_T) = \prod_{t=1}^T p(x_t | x_1, \dots, x_{t-1}) \quad (6)$$

This results in a history-dependent representation vector  $\vec{h}_t^{(l)}$  given its history context  $(x_1, \dots, x_{t-1})$ . In the even-indexed layers  $l \in \{2, 4, \dots, L\}$ , the backward model runs over the sequence  $x$  in reverse, predicting a previous timestep  $x_t$  given the future context  $(x_{t+1}, \dots, x_T)$ :

$$p(x_1, x_2, \dots, x_T) = \prod_{t=1}^T p(x_t | x_{t+1}, \dots, x_T) \quad (7)$$

This yields a future-dependent representation vector  $\overleftarrow{h}_t^{(l)}$  given its future context  $(x_{t+1}, \dots, x_T)$ . The conditional probabilities in Equation (6) and Equation (7) can be modeled by forward and backward attention (Radford & Narasimhan, 2018).

Figure 3.b illustrates how the BAAR framework alternates between forward and backward layers to learn deep bidirectional representations. In the odd-indexed layer, the forward attention starts with a [SOS] token to predict the next tokens from left to right, where the [EOS] token summarizes information from all timesteps. In the even-indexed layer, the backward attention begins with the [EOS] token to predict the previous token in the right-to-left direction, intending to reconstruct the sequence in reverse. By alternating left-to-right and right-to-left information flows, the [EOS] and [SOS] tokens aggregate the sequence’s features in the odd and even layers, respectively. In the final layer (assuming  $L$  is an even number), the [SOS] token serves as a sequence representation for discriminative tasks.

### 3.2. BiTimelyGPT Architecture

As shown in Figure 3.c, BiTimelyGPT employs the BAAR framework to alternately model left-to-right and right-to-left information flows across layers. In the odd-indexed layers  $l \in \{1, 3, \dots, L-1\}$ , BiTimelyGPT utilizes a forward retention to model left-to-right information with Equation (4), where the lower triangular decay matrix  $\vec{D}$  maintains this direction. In the even-indexed layers  $l = (2, 4, \dots, L)$ , BiTimelyGPT utilizes a backward retention to model right-to-left information:

$$\overleftarrow{\text{Ret}}(\mathbf{X}) = \underbrace{(\hat{\mathbf{Q}}\hat{\mathbf{K}}^\top \odot \overleftarrow{\mathbf{D}})}_{\overleftarrow{\mathbf{R}}} \mathbf{V}, \quad \overleftarrow{\mathbf{D}}_{nm} = \begin{cases} \gamma^{m-n}, & n \leq m \\ 0, & n > m \end{cases} \quad (8)$$

where an upper triangular decay matrix  $\overleftarrow{\mathbf{D}}$  maintains right-to-left direction. Consequently, BiTimelyGPT alternates between forward and backward retention across layers, pre-training deep bidirectional representations.

In BiTimelyGPT, bidirectional generative pre-training aims to learn deep bidirectional representations from unlabeled data, preserving the original distribution and time-series shapelets without any data alterations. To maximize the joint probability of observing the entire sequence, BiTimelyGPT predicts the next token in the Layer  $L-1$  and the previous token in the Layer  $L$ , respectively. We define the objective of Next-Previous-Token Prediction task as follows.

$$\sum_{t=1}^T \log p(x_t^{(L-1)} | x_1^{(L-1)}, \dots, x_{t-1}^{(L-1)}) + \log p(x_t^{(L)} | x_{t+1}^{(L)}, \dots, x_T^{(L)}) \quad (9)$$

The output projection layer takes each token’s representations  $\vec{h}_t^{(L-1)}$  and  $\overleftarrow{h}_t^{(L)}$  to predict the next and previous tokens, respectively. The pre-training loss is mean squared error (MSE) for continuous signals (e.g., biosignal) or cross-entropy for discrete signals (e.g., diagnosis codes). The [SOS] token in the final layer is used for fine-tuning as it aggregates a sequence representation for downstream tasks.

### 3.3. Full-rankedness in BiTimelyGPT

The self-attention mechanism often suffers from the low-rank bottleneck, leading to a loss of expressiveness in the rank-deficient attention matrix  $\overleftrightarrow{\mathbf{A}}$  (Dong et al., 2021; Bhojanapalli et al., 2020). For single-head attention in Equation (1), when the dimension  $d$  is less than the sequence length  $N$ , we have  $\text{rank}(\mathbf{Q}\mathbf{K}^\top) \leq d$ , resulting in a rank-deficient  $\overleftrightarrow{\mathbf{A}} \in \mathbb{R}^{N \times N}$  without Softmax activation. This bottleneck persists even with non-linear Softmax operation (Wang et al., 2020; Zhang et al., 2022b). This challenge is exacerbated in multi-head attention, where the dimension per head is much smaller than  $N$  (Bhojanapalli et al.,

Table 1. Model comparison from various perspectives. BiTimelyGPT achieves data preservation, bidirectionality, and full-rankedness.

Model	Pre-training	Data Preservation	Bidirectionality	Full-rankedness
PatchTST	Masking-based	✗	✓	✗
CRT	Dropping-based	✗	✓	✗
TimelyGPT	Next-Token Prediction	✓	✗	✓
TimelyBERT	Masking-based	✗	✓	✗
<b>BiTimelyGPT</b>	Next-Previous-Token Prediction	✓	✓	✓

2020). In contrast, GPT’s masked attention matrix  $\vec{A}$  in Equation (2) is full-rank (i.e.,  $\det(\vec{A}) \neq 0$ ), forming a lower triangular matrix with strictly positive diagonal elements post-Softmax activation. Although this full-rank matrix  $\vec{A}$  offers expressive representation power, it is limited to unidirectional contexts.

BiTimelyGPT effectively overcomes the low-rank bottleneck by alternating between forward and backward retention, resulting in triangular retention matrices with non-zero diagonals. Specifically, the forward retention matrix  $\vec{R}$  in Equation (4) becomes full-rank when its diagonal elements are non-zero, ensuring  $\det(\vec{R}) \neq 0$ . For a diagonal element  $\vec{R}_{mm} = \mathbf{W}_Q \mathbf{X}_m (\mathbf{W}_K \mathbf{X}_m)^\top$ , this condition is satisfied by initializing these embeddings to prevent orthogonality and avoid all-zeros across the  $d$  dimensions. This reasoning also applies to the backward retention  $\overleftarrow{R}$  in Equation (8). Consequently, both forward and backward retention matrices in BiTimelyGPT are full-rank, enabling to learn bidirectional contexts using more expressive attention matrices.

## 4. Experiment

### 4.1. Experiment Design

To evaluate BiTimelyGPT, we conducted both qualitative and quantitative analyses. Qualitatively, we visualized and interpreted three key advantages of BiTimelyGPT: data preservation during pre-training (Section 4.2), bidirectionality (Section 4.3), and full-rankedness (Section 4.4). For the quantitative analysis in Section 4.5, we assessed the performance of BiTimelyGPT on discriminative classification and regression tasks against a broad range of baseline models.

**Datasets.** We used three publicly available, large-scale time-series datasets for pre-training: (1) the Sleep-EDF dataset with 7 types of biosignals across 1.2 billion timesteps (Kemp et al., 2000); (2) the PTB-XL dataset with 12 types of electrocardiogram data totaling 109 million timesteps (Alday et al., 2020); (3) the PPG-Dalia dataset with 4 types of photoplethysmograph data from 16.6 million timesteps (Reiss et al., 2019a). Additionally, we employed five other datasets for downstream discriminative tasks, namely Epilepsy (Andrzejak et al., 2001), EMG (Goldberger et al.,

2000), RR, HR, SpO2 (Tan et al., 2021). The description and statistics of datasets are available in Appendix B.1.

**Qualitative Analysis Design.** We conducted visualization analyses using the large-scale Sleep-EDF dataset, including (1) the gradient-based saliency for data preservation during generative pre-training; (2) the attention matrices for bidirectionality effectiveness; (3) the rank analysis of attention matrices for model expressiveness. To ensure consistency in comparison, we used the same patch-tokenizer with a non-overlapping patch size of 8, yielding  $N = 375$  tokens per 3000-timestep sequence (Nie et al., 2023).

**Quantitative Experiment Design.** For classification, we pre-trained on the Sleep-EDF and PTB-XL datasets separately. Subsequently, the PTMs were fine-tuned on the Sleep-EDF, Epilepsy, PTB-XL, and EMG datasets. For regression, we pre-trained on both the PTB-XL and PPGDalia datasets, and then fine-tuned PTMs on the IEEPPG, RR, HR, and SpO2 datasets. We divided each dataset into training (80%), validation (10%), and test (10%) sets. When the same dataset was used for both pre-training and fine-tuning, we fine-tuned the PTMs using 20% of the training set. All models adopted the preferred tokenization setup. We used accuracy and MAE as metrics for classification and regression, respectively.

**Pre-training and Fine-tuning.** BiTimelyGPT performed pre-training with Next-Previous-Token Prediction task, with fine-tuning on the [SOS] token in the final layer. PatchTST adopted a masking-based approach, masking 40% of its patches as zero (Nie et al., 2023). CRT utilized a dropping-based pre-training, discarding up to 70% of patches (Zhang et al., 2023). For transformers without established pre-training methods, we used a masking-based method by randomly masking 40% of timesteps (Zerveas et al., 2021). All transformers performed 20 epochs of pre-training with MSE loss, followed by 5 epochs of end-to-end fine-tuning.

**Bidirectional TimelyBERT Baseline.** We also evaluated an intuitive baseline TimelyBERT, which uses bidirectional retention matrix  $\overleftrightarrow{R}$  in each layer. This baseline modifies the decay matrix as  $\overleftrightarrow{D} = \gamma^{|n-m|}$  in Equation (10). However, the TimelyBERT baseline faces two limitations: (1) this encoder-only model utilizes masking-based pre-training,

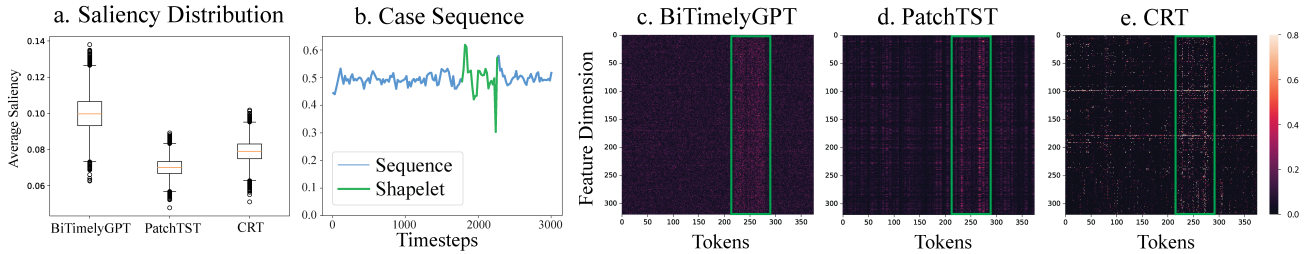


Figure 4. Visualization of different pre-training methods. **a.** Distribution of average saliency scores within the extracted shaplets of sequences. **b.** A case example of time-series and its shapelet. **c.** Generative pre-training of BiTimelyGPT. The green rectangle indicates the shapelet discriminative region. **d.** Masking-based pre-training of PatchTST. **e.** Dropping-based pre-training of CRT.

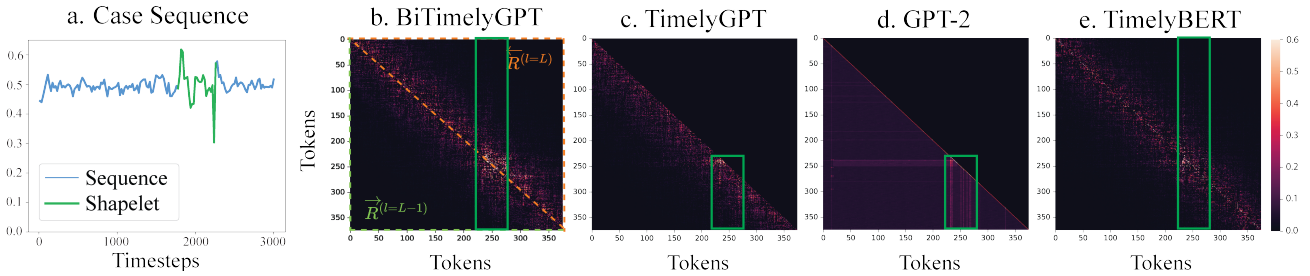


Figure 5. Visualization of bidirectionality advantage for a discriminative shaplet. **a.** A case example of time-series and its data shapelet. **b.** The combined retention matrices from the last two layers of BiTimelyGPT. The green rectangle indicates the shapelet discriminative region. **c.** TimelyGPT’s causal retention matrix. **d.** GPT-2’s causal attention matrix. **e.** TimelyBERT’s bidirectional retention matrix.

resulting in distribution shift; (2) its bidirectional retention  $\overleftarrow{\mathbf{R}}$  suffers from the low-rank bottleneck:

$$\overleftarrow{\text{Ret}}(\mathbf{X}) = \underbrace{(\hat{\mathbf{Q}}\hat{\mathbf{K}}^\top \odot \overleftarrow{\mathbf{D}})}_{\overleftarrow{\mathbf{R}}} \mathbf{V}, \quad \overleftarrow{\mathbf{D}}_{nm} = \gamma^{|n-m|} \quad (10)$$

## 4.2. Visualization of Different Pre-training Strategies

We examined the impact of different pre-training methods on representation learning with respect to data preservation, focusing on BiTimelyGPT, masking-based PatchTST, and dropping-based CRT. We assessed the saliency of the  $N \times d$  output embedding matrix generated during pre-training by computing the absolute value of the corresponding gradients with respect to the prediction target (Wagner & Foster, 2023). To identify discriminative patterns in time-series data (Ye & Keogh, 2009; Grabocka et al., 2014), we extracted shapelets from 10% of the Sleep-EDF dataset using the pyts package (Faouzi & Janati, 2020), followed by computing the average saliency values within these positions.

As shown in Figure 4.a, BiTimelyGPT had higher saliency scores on the regions of data shapelets, suggesting its superior ability to uncover discriminative patterns compared to the baselines. Furthermore, we conducted a case study on a specific sequence with a distinct shapelet (Figure 4.b).

The saliency heatmap of the output embedding matrix (Figure 4.c) revealed that BiTimelyGPT efficiently captured discriminative information surrounding the shapelet. In comparison, PatchTST (Figure 4.d) and CRT (Figure 4.e) displayed high saliency beyond the region of shapelet driven by the minimization of the reconstruction loss, failing to concentrate on discriminative patterns. These observations underscore that BiTimelyGPT’s pre-training effectively discerns discriminative information compared to masking-based and dropping-based approaches.

## 4.3. Visualization of Bidirectionality

We investigated the effectiveness of bidirectionality in attention matrices on a downstream classification task. Through a case study in Figure 5, we compared the attention matrices from fine-tuned models of BiTimelyGPT, TimelyGPT (Song et al., 2023), GPT-2 (Radford et al., 2019), and TimelyBERT. For BiTimelyGPT (Figure 5.b), we combined its lower and upper triangular retention matrices,  $\overleftarrow{\mathbf{R}}^{L-1}$  and  $\overrightarrow{\mathbf{R}}^L$ , to demonstrate its bidirectional representations. Our analysis showed that BiTimelyGPT exhibited localized and concentrated attention on the key discriminative region, efficiently integrating bidirectional contexts. In contrast, TimelyGPT (Figure 5.c) exhibit more limited focus on the discriminative

Table 2. Compare BiTimelyGPT against various baselines for downstream seq2vec tasks. Best values are highlighted in bold.

Task	Classification (Accuracy %)				Regression (MAE)			
Pre-training	Sleep-EDF		PTB-XL		PTB-XL & PPGDalia			
Fine-tuning	Sleep-EDF	Epilepsy	PTB-XL	EMG	IEEEPPG	RR	HR	SpO2
BiTimelyGPT	<b>90.41</b>	<b>93.02</b>	87.47	<b>95.36</b>	26.11	2.81	<b>8.42</b>	<b>4.23</b>
TimelyGPT	89.21	92.79	86.52	95.87	26.17	<b>2.78</b>	8.53	4.26
TimelyGPT w/o Conv	85.32	90.45	84.51	93.26	27.32	3.03	8.92	4.55
TimelyBERT	82.17	85.64	81.03	84.52	30.96	4.22	12.86	4.82
CRT	90.12	91.05	<b>87.81</b>	94.56	26.52	2.96	9.02	4.48
PatchTST	89.57	91.27	83.42	95.23	<b>26.08</b>	2.89	9.46	4.45
AutoFormer	78.86	84.21	78.51	88.56	32.18	4.13	13.29	4.95
FedFormer	76.43	81.65	75.53	85.21	31.11	4.36	13.82	4.75
TimesNet	83.58	85.96	79.38	89.26	29.95	4.19	13.65	4.83
TST	88.83	88.02	81.86	94.16	26.81	3.47	12.63	4.95
GPT	84.25	88.65	83.11	92.58	28.62	3.71	11.09	4.64
GPT-BAAR	86.17	89.73	85.09	93.71	28.17	3.60	10.62	4.66
TS2Vec	86.21	88.27	82.65	93.77	27.89	3.53	11.56	4.60
TS-TCC	86.06	89.74	84.66	93.25	29.32	4.09	13.64	4.86
TF-C	86.56	87.52	82.71	93.83	28.52	4.38	14.15	4.87
LSTM	80.15	76.51	78.83	86.95	30.15	4.95	14.37	5.05
LSTM-BAAR	82.22	81.05	82.30	87.96	28.06	4.53	11.78	4.82
BiLSTM	81.63	78.32	80.72	86.84	29.43	4.71	13.50	4.97
ELMo	82.15	81.60	80.98	88.52	28.15	4.66	12.42	4.76

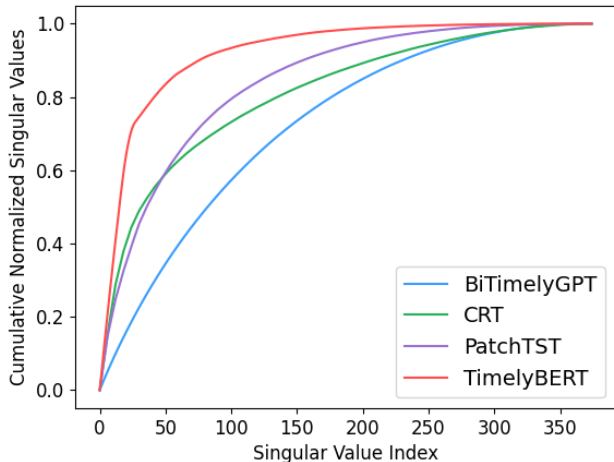


Figure 6. Normalized cumulative singular values of the attention matrices. A more uniformly distributed curve of singular values, indicates a higher rank of the corresponding attention matrix.

segment. GPT-2 (Figure 5.d) had a broader but less precise range of attention around these key features. TimelyBERT (Figure 5.e), despite having decay mechanisms in both directions, struggled to concentrate attention on the discriminative regions. These findings highlight the effectiveness of BiTimelyGPT in identifying discriminative patterns through its modeling of bidirectional contextualized representations.

#### 4.4. Visualization of Attention Matrix Rankness

We assessed the expressiveness of the attention matrices in various bidirectional transformers, including BiTimelyGPT, PatchTST, CRT, and TimelyBERT. We applied singular value decomposition (SVD) to the attention matrices across different layers and heads, visualizing the normalized cumulative singular values in Figure 6. Our analysis revealed that BiTimelyGPT conferred a more uniform distribution of singular values, effectively overcoming the low-rank bottleneck. In contrast, the singular value curves for other bidirectional baselines skewed towards the upper left corner, suggesting that a few largest singular values can account for most information in the attention matrices. Notably, TimelyBERT had the most long-tail spectrum distribution, due to its retention matrix  $\vec{R} = \vec{Q}\vec{K}^\top \odot \vec{D}$  lacking softmax’s non-linearity. As a result, BiTimelyGPT demonstrated more expressive representation power, breaking the low-rank bottleneck common in other bidirectional transformers.

#### 4.5. Performance on seq2vec Fine-Tuning Tasks

**Baselines.** For the classification and regression supervised fine-tuning tasks, we compared BiTimelyGPT against a broad range of baselines, including transformer PTMs, consistency-based PTMs, and recurrent models. Among transformer models, we included TimelyGPT, TimelyBERT,

Table 3. Ablation results of BiTimelyGPT w/o specific components in terms of downstream Sleep-EDF classification accuracy.

Method / Classification	Sleep-EDF
<b>BiTimelyGPT</b> (Generative Pre-training)	90.41
w/o BAAR	87.65
w/o xPos (i.e., GPT-2)	84.25
BiTimelyGPT(w/o Pre-training)	86.33

CRT, PatchTST, AutoFormer (Wu et al., 2021), FedFormer (Zhou et al., 2022), TST (Zerveas et al., 2021), and TimesNet (Wu et al., 2023). Consistency-based PTMs such as TS-TCC (Eldele et al., 2021), TS2Vec (Yue et al., 2022), and TF-C (Zhang et al., 2022a) were also evaluated; these models focus on learning effective representations by optimizing the distance between representations of positive and negative pairs via contrastive learning (Ma et al., 2023). We also assessed recurrent models like LSTM, BiLSTM, and ELMo. Additionally, to explore the efficacy of our proposed BAAR framework, we applied it to other autoregressive models GPT-2 and LSTM. We describe the architectures and parameters for BiTimelyGPT and baselines in Appendix B.2.

**Results.** As shown in Table 2, BiTimelyGPT demonstrated the best performance in the classification on Sleep-EDF, Epilepsy and EMG datasets and the regression on HR and SpO2 datasets. These results highlight the effectiveness of BiTimelyGPT’s bidirectionality, surpassing unidirectional TimelyGPT enhanced with convolution. Additionally, the data preservation during pre-training and full-rank retention matrices contributed considerably to BiTimelyGPT’s superior performance over other bidirectional transformers. CRT, employing a dropping-based pre-training, performed consistently well across datasets and achieved top results in the PTB-XL dataset. In contrast, masking-based PTMs typically lagged behind due to the distribution shift. Among these masking-based PTMs, Autoformer, Fedformer, and TimesNet, which rely heavily on time decomposition and frequency-domain information, were especially affected by distribution shift. This suggests the advantage of dropping-based pre-training regime in avoiding distribution shift over the masking-based pre-training methods. Furthermore, both consistency-based PTMs and recurrent models showed inferior performance in these tasks. The applications of the BAAR framework to GPT and LSTM resulted in improved performance, indicating its broad adaptability and effectiveness in enhancing various autoregressive models.

## 5. Ablation Study

To evaluate the contributions of various components in BiTimelyGPT, we conducted ablation studies by selectively **omitting** bidirectionality and xPos embedding. We focused on the pre-training and fine-tuning on the Sleep-EDF

Table 4. Probing study for the selection of sentence representations for downstream Sleep-EDF classification.

Sequence Representation	Sleep-EDF
<b>[SOS]</b> ( $l = L$ )	90.41
[EOS] ( $l = L$ )	89.66
[SOS] + [EOS] ( $l = L$ )	90.11
All ( $l = L$ )	90.15
[SOS] ( $l = \{L - 1, L\}$ )	88.63
[EOS] ( $l = L$ )	89.52
[SOS] + [EOS] ( $l = \{L - 1, L\}$ )	89.22
All ( $l = \{L - 1, L\}$ )	89.62

dataset for classification. In Table 3, the xPos embedding increased performance by 3.40% by effectively encoding extrapolatable temporal patterns into time-series representations. The integration of the BAAR framework allows BiTimelyGPT to learn deep bidirectional representations, improving the downstream seq2vec tasks by 2.76%.

## 6. Probing Study

We also explored the most effective choice of sequence features for downstream tasks (Table 4). Focusing on the last layer ( $l = L$ ) and the last two layers ( $l = \{L - 1, L\}$ ), we examined four token combinations: [SOS] token alone, [EOS] token alone, both [SOS] and [EOS] tokens, and all tokens. In cases with multiple tokens, we applied average pooling for sequence representation. We observed that the [SOS] token from the last layer is sufficient to achieve the best Sleep-EDF classification, attributed to its aggregation of sequence information by backward attention.

## 7. Conclusion and Future Work

We present a BiTimelyGPT model, which leverages the recurrent attention and BAAR framework, for time-series representation learning and downstream discriminative tasks. Extensive visualization analyses underscore BiTimelyGPT’s three contributions: (1) the Next-Previous-Token Prediction pre-training effectively preserves the original distribution and data shapelets; (2) the BAAR framework alternates forward and backward retention across layers, learning deep bidirectional representations; (3) the full-rank forward and backward retention matrices enhance representation expressiveness. Empirical results demonstrate BiTimelyGPT’s superiority in the classification and regression on eight widely-used datasets. For future work, we would adapt BiTimelyGPT for out-of-distribution biosignals, further enhancing its utility in healthcare time-series. Additionally, we will broaden the applicability of BiTimelyGPT across multiple domains and data modalities, and experiment the benefits of BAAR framework with various autoregressive models.



## References

- Alday, E. A. P., Gu, A., Shah, A. J., Robichaux, C., Wong, A.-K. I., Liu, C., Liu, F., Rad, A. B., Elola, A., Seyedi, S., Li, Q., Sharma, A., Clifford, G. D., and Reyna, M. A. Classification of 12-lead eegs: the physionet/computing in cardiology challenge. *Physiological measurement*, 41: 124003, 2020. doi: 10.1088/1361-6579/abc960.
- Andrzejak, R. G., Lehnertz, K., Mormann, F., Rieke, C., David, P., and Elger, C. E. Indications of nonlinear deterministic and finite-dimensional structures in time series of brain electrical activity: Dependence on recording region and brain state. *Physical review. E, Statistical, nonlinear, and soft matter physics*, 6:061907, 2001.
- Bengio, Y., Ducharme, R., and Vincent, P. A neural probabilistic language model. In Leen, T., Dietterich, T., and Tresp, V. (eds.), *Advances in Neural Information Processing Systems*, volume 13. MIT Press, 2000. URL [https://proceedings.neurips.cc/paper\\_files/paper/2000/file/728f206c2a01bf572b5940d7d9a8fa4c-Paper.pdf](https://proceedings.neurips.cc/paper_files/paper/2000/file/728f206c2a01bf572b5940d7d9a8fa4c-Paper.pdf).
- Bhojanapalli, S., Yun, C., Rawat, A. S., Reddi, S., and Kumar, S. Low-rank bottleneck in multi-head attention models. In III, H. D. and Singh, A. (eds.), *Proceedings of the 37th International Conference on Machine Learning*, volume 119 of *Proceedings of Machine Learning Research*, pp. 864–873. PMLR, 13–18 Jul 2020. URL <https://proceedings.mlr.press/v119/bhojanapalli20a.html>.
- Devlin, J., Chang, M.-W., Lee, K., and Toutanova, K. BERT: Pre-training of deep bidirectional transformers for language understanding. In Burstein, J., Doran, C., and Solorio, T. (eds.), *Proceedings of the 2019 Conference of the North American Chapter of the Association for Computational Linguistics: Human Language Technologies, Volume 1 (Long and Short Papers)*, pp. 4171–4186, Minneapolis, Minnesota, June 2019. Association for Computational Linguistics. doi: 10.18653/v1/N19-1423. URL <https://aclanthology.org/N19-1423>.
- Dong, Y., Cordonnier, J.-B., and Loukas, A. Attention is not all you need: pure attention loses rank doubly exponentially with depth. In Meila, M. and Zhang, T. (eds.), *Proceedings of the 38th International Conference on Machine Learning*, volume 139 of *Proceedings of Machine Learning Research*, pp. 2793–2803. PMLR, 18–24 Jul 2021. URL <https://proceedings.mlr.press/v139/dong21a.html>.
- Dosovitskiy, A., Beyer, L., Kolesnikov, A., Weissenborn, D., Zhai, X., Unterthiner, T., Dehghani, M., Minderer, M., Heigold, G., Gelly, S., Uszkoreit, J., and Houlsby, N. An image is worth 16x16 words: Transformers for image recognition at scale. In *9th International Conference on Learning Representations, ICLR 2021, Virtual Event, Austria, May 3-7, 2021*. OpenReview.net, 2021. URL <https://openreview.net/forum?id=YicbFdNTTy>.
- Eldele, E., Ragab, M., Chen, Z., Wu, M., Kwok, C. K., Li, X., and Guan, C. Time-series representation learning via temporal and contextual contrasting. In *Proceedings of the Thirtieth International Joint Conference on Artificial Intelligence, IJCAI-21*, pp. 2352–2359, 2021.
- Faouzi, J. and Janati, H. pyts: A python package for time series classification. *Journal of Machine Learning Research*, 21(46):1–6, 2020. URL <http://jmlr.org/papers/v21/19-763.html>.
- Goldberger, A., Amaral, L., Glass, L., Hausdorff, J., Ivanov, P., Mark, R., Mietus, J., Moody, G., Peng, C., and Stanley, H. Physiobank, physiotoolkit, and physionet: components of a new research resource for complex physiologic signals. *Circulation*, 101(23):e215–e220, 2000. doi: 0.1161/01.cir.101.23.e215.
- Grabocka, J., Schilling, N., Wistuba, M., and Schmidt-Thieme, L. Learning time-series shapelets. In *Proceedings of the 20th ACM SIGKDD International Conference on Knowledge Discovery and Data Mining, KDD '14*, pp. 392–401, New York, NY, USA, 2014. Association for Computing Machinery. ISBN 9781450329569. doi: 10.1145/2623330.2623613. URL <https://doi.org/10.1145/2623330.2623613>.
- Gulati, A., Qin, J., Chiu, C.-C., Parmar, N., Zhang, Y., Yu, J., Han, W., Wang, S., Zhang, Z., Wu, Y., and Pang, R. Conformer: Convolution-augmented transformer for speech recognition. pp. 5036–5040, 10 2020. doi: 10.21437/Interspeech.2020-3015.
- Kemp, B., Zwinderman, A., Tuk, B., Kamphuisen, H., and Obery, J. Analysis of a sleep-dependent neuronal feedback loop: the slow-wave microcontinuity of the eeg. *IEEE Transactions on Biomedical Engineering*, 47(9): 1185–1194, 2000. doi: 10.1109/10.867928.
- Ma, Q., Liu, Z., Zheng, Z., Huang, Z., Zhu, S., Yu, Z., and Kwok, J. T. A survey on time-series pre-trained models, 2023.
- Nie, Y., H. Nguyen, N., Sinthong, P., and Kalagnanam, J. A time series is worth 64 words: Long-term forecasting with transformers. In *International Conference on Learning Representations*, 2023.
- Peters, M. E., Neumann, M., Iyyer, M., Gardner, M., Clark, C., Lee, K., and Zettlemoyer, L. Deep contextualized word representations. In Walker, M., Ji, H.,

- and Stent, A. (eds.), *Proceedings of the 2018 Conference of the North American Chapter of the Association for Computational Linguistics: Human Language Technologies, Volume 1 (Long Papers)*, pp. 2227–2237, New Orleans, Louisiana, June 2018. Association for Computational Linguistics. doi: 10.18653/v1/N18-1202. URL <https://aclanthology.org/N18-1202>.
- Phan, H., Chen, O. Y., Tran, M. C., Koch, P., Mertins, A., and Vos, M. D. XSleepNet: Multi-view sequential model for automatic sleep staging. *IEEE Transactions on Pattern Analysis and Machine Intelligence*, pp. 1–1, 2021. doi: 10.1109/tpami.2021.3070057. URL <https://doi.org/10.1109%2Ftpami.2021.3070057>.
- Pimentel, M. A. F., Johnson, A. E. W., Charlton, P. H., Birrenkott, D., Watkinson, P. J., Tarassenko, L., and Clifton, D. A. Toward a robust estimation of respiratory rate from pulse oximeters. *IEEE Transactions on Biomedical Engineering*, 64(8):1914–1923, 2017. doi: 10.1109/TBME.2016.2613124.
- Radford, A. and Narasimhan, K. Improving language understanding by generative pre-training. 2018. URL <https://api.semanticscholar.org/CorpusID:49313245>.
- Radford, A., Wu, J., Child, R., Luan, D., Amodei, D., and Sutskever, I. Language models are unsupervised multitask learners. 2019.
- Radford, A., Kim, J. W., Hallacy, C., Ramesh, A., Goh, G., Agarwal, S., Sastry, G., Askell, A., Mishkin, P., Clark, J., Krueger, G., and Sutskever, I. Learning transferable visual models from natural language supervision. In Meila, M. and Zhang, T. (eds.), *Proceedings of the 38th International Conference on Machine Learning, ICML 2021, 18-24 July 2021, Virtual Event*, volume 139 of *Proceedings of Machine Learning Research*, pp. 8748–8763. PMLR, 2021. URL <http://proceedings.mlr.press/v139/radford21a.html>.
- Reiss, A., Indlekofer, I., Schmidt, P., and Laerhovenn, K. V. Deep ppg: Large-scale heart rate estimation with convolutional neural networks. *Sensors*, 19(14):3079, 2019a. doi: 10.3390/s19143079.
- Reiss, A., Indlekofer, I., Schmidt, P., and Van Laerhoven, K. Deep ppg: Large-scale heart rate estimation with convolutional neural networks. *Sensors*, 19(14), 2019b. ISSN 1424-8220. doi: 10.3390/s19143079. URL <https://www.mdpi.com/1424-8220/19/14/3079>.
- Song, Z., Lu, Q., Xu, H., and Li, Y. Timelygpt: Recurrent convolutional transformer for long time-series representation, 2023.
- Stirling, R., Cook, M., Grayden, D., and Karoly, P. Seizure forecasting and cyclic control of seizures. *Epilepsia*, 62 Suppl 1, 07 2020. doi: 10.1111/epi.16541.
- Sun, Y., Dong, L., Huang, S., Ma, S., Xia, Y., Xue, J., Wang, J., and Wei, F. Retentive network: A successor to transformer for large language models, 2023a.
- Sun, Y., Dong, L., Patra, B., Ma, S., Huang, S., Benhaim, A., Chaudhary, V., Song, X., and Wei, F. A length-extrapolatable transformer. In Rogers, A., Boyd-Graber, J., and Okazaki, N. (eds.), *Proceedings of the 61st Annual Meeting of the Association for Computational Linguistics (Volume 1: Long Papers)*, pp. 14590–14604, Toronto, Canada, July 2023b. Association for Computational Linguistics. doi: 10.18653/v1/2023.acl-long.816. URL <https://aclanthology.org/2023.acl-long.816>.
- Tan, C. W., Bergmeir, C., Petitjean, F., and Webb, G. I. Time series extrinsic regression. *Data Mining and Knowledge Discovery*, pp. 1–29, 2021. doi: <https://doi.org/10.1007/s10618-021-00745-9>.
- Vaswani, A., Shazeer, N., Parmar, N., Uszkoreit, J., Jones, L., Gomez, A. N., Kaiser, L. u., and Polosukhin, I. Attention is all you need. In Guyon, I., Luxburg, U. V., Bengio, S., Wallach, H., Fergus, R., Vishwanathan, S., and Garnett, R. (eds.), *Advances in Neural Information Processing Systems*, volume 30. Curran Associates, Inc., 2017. URL [https://proceedings.neurips.cc/paper\\_files/paper/2017/file/3f5ee243547dee91fbd053c1c4a845aa-Paper.pdf](https://proceedings.neurips.cc/paper_files/paper/2017/file/3f5ee243547dee91fbd053c1c4a845aa-Paper.pdf).
- Wagner, J. and Foster, J. Investigating the saliency of sentiment expressions in aspect-based sentiment analysis. In Rogers, A., Boyd-Graber, J., and Okazaki, N. (eds.), *Findings of the Association for Computational Linguistics: ACL 2023*, pp. 12751–12769, Toronto, Canada, July 2023. Association for Computational Linguistics. doi: 10.18653/v1/2023.findings-acl.807. URL <https://aclanthology.org/2023.findings-acl.807>.
- Wang, S., Li, B. Z., Khabsa, M., Fang, H., and Ma, H. Linformer: Self-attention with linear complexity, 2020.
- Wu, H., Xu, J., Wang, J., and Long, M. Autoformer: Decomposition transformers with auto-correlation for long-term series forecasting. *CoRR*, abs/2106.13008, 2021. URL <https://arxiv.org/abs/2106.13008>.
- Wu, H., Hu, T., Liu, Y., Zhou, H., Wang, J., and Long, M. Timesnet: Temporal 2d-variation modeling for general time series analysis. In *International Conference on Learning Representations*, 2023.

- Ye, L. and Keogh, E. Time series shapelets: A new primitive for data mining. In *Proceedings of the 15th ACM SIGKDD International Conference on Knowledge Discovery and Data Mining*, KDD '09, pp. 947–956, New York, NY, USA, 2009. Association for Computing Machinery. ISBN 9781605584959. doi: 10.1145/1557019.1557122. URL <https://doi.org/10.1145/1557019.1557122>.
- Yue, Z., Wang, Y., Duan, J., Yang, T., Huang, C., Tong, Y., and Xu, B. Ts2vec: Towards universal representation of time series. *Proceedings of the AAAI Conference on Artificial Intelligence*, 36:8980–8987, Jun. 2022. doi: 10.1609/aaai.v36i8.20881. URL <https://ojs.aaai.org/index.php/AAAI/article/view/20881>.
- Zerveas, G., Jayaraman, S., Patel, D., Bhamidipaty, A., and Eickhoff, C. A transformer-based framework for multivariate time series representation learning. In *Proceedings of the 27th ACM SIGKDD Conference on Knowledge Discovery & Data Mining*, KDD '21, pp. 2114–2124, New York, NY, USA, 2021. Association for Computing Machinery. ISBN 9781450383325. doi: 10.1145/3447548.3467401. URL <https://doi.org/10.1145/3447548.3467401>.
- Zhang, W., Yang, L., Geng, S., and Hong, S. Self-supervised time series representation learning via cross reconstruction transformer. *IEEE Transactions on Neural Networks and Learning Systems*, pp. 1–10, 2023. doi: 10.1109/TNNLS.2023.3292066.
- Zhang, X., Zhao, Z., Tsiligkaridis, T., and Zitnik, M. Self-supervised contrastive pre-training for time series via time-frequency consistency. In *Proceedings of Neural Information Processing Systems, NeurIPS*, 2022a.
- Zhang, Z., Pi, Z., and Liu, B. Troika: A general framework for heart rate monitoring using wrist-type photoplethysmographic signals during intensive physical exercise. *IEEE Transactions on Biomedical Engineering*, 62(2):522–531, 2015. doi: 10.1109/TBME.2014.2359372.
- Zhang, Z., Shao, N., Gao, C., Miao, R., Yang, Q., and Shao, J. Mixhead: Breaking the low-rank bottleneck in multi-head attention language models. *Know.-Based Syst.*, 240(C), mar 2022b. ISSN 0950-7051. doi: 10.1016/j.knosys.2021.108075. URL <https://doi.org/10.1016/j.knosys.2021.108075>.
- Zhou, T., Ma, Z., Wen, Q., Wang, X., Sun, L., and Jin, R. FEDformer: Frequency enhanced decomposed transformer for long-term series forecasting. In *Proc. 39th International Conference on Machine Learning (ICML 2022)*, 2022.

## A. Additional Information for BiTimelyGPT

### A.1. Denotations of Variables

Table 5. Notations in BiTimelyGPT

Notations	Descriptions	Notations	Descriptions
$T$	Number of timesteps in a time-series	$N$	Number of tokens
$V$	Number of variates	$L$	Number of layers
$d$	The hidden dimension	$h$	Number of heads
$x \in \mathbb{R}^{T \times V}$	A time-series sequence	$\mathbf{X} \in \mathbb{R}^{N \times d}$	A sequence of tokens
[SOS]	The start token of a sequence	[EOS]	The end token of a sequence
$\mathbf{Q}, \mathbf{K}, \mathbf{V} \in \mathbb{R}^{N \times d}$	The query, key, value matrices	$\mathbf{W}_Q, \mathbf{W}_K, \mathbf{W}_V \in \mathbb{R}^{d \times d}$	The projection matrices for $\mathbf{Q}, \mathbf{K}, \mathbf{V}$
$\overleftrightarrow{\mathbf{A}} \in \mathbb{R}^{N \times N}$	The bidirectional attention matrix	$\overrightarrow{\mathbf{A}} \in \mathbb{R}^{N \times N}$	The forward attention matrix
$\mathbf{C} \in \mathbb{R}^{N \times N}$	The lower triangular mask matrix	$\mathbf{S} \in \mathbb{R}^{d \times d}$	The state variable for retention
$\overleftarrow{\mathbf{Q}}, \overleftarrow{\mathbf{K}}, \overleftarrow{\mathbf{V}} \in \mathbb{R}^{N \times d}$	$\mathbf{Q}, \mathbf{K}, \mathbf{V}$ with xPos embedding	$\overleftarrow{\mathbf{Q}}, \overleftarrow{\mathbf{K}}, \overleftarrow{\mathbf{V}} \in \mathbb{R}^{N \times d}$	$\mathbf{Q}, \mathbf{K}, \mathbf{V}$ with RoPE embedding
$\theta$	The rotary angle hyperparameter	$\gamma$	The exponential decay hyperparameter
$\overrightarrow{\mathbf{R}} \in \mathbb{R}^{N \times N}$	The forward retention matrix	$\overleftarrow{\mathbf{D}} \in \mathbb{R}^{N \times N}$	The lower triangular decay matrix
$\overleftarrow{\mathbf{R}} \in \mathbb{R}^{N \times N}$	The backward retention matrix	$\overrightarrow{\mathbf{D}} \in \mathbb{R}^{N \times N}$	The upper triangular decay matrix
$\overleftrightarrow{\mathbf{R}} \in \mathbb{R}^{N \times N}$	The bidirectional retention matrix	$\overleftrightarrow{\mathbf{D}} \in \mathbb{R}^{N \times N}$	The bidirectional decay matrix

### A.2. BiTimelyGPT Pre-training overview

Figure 7 depicts the process of input processing followed by Next-Previous-Token Prediction pre-training. The input of time-series sequence with  $T$  timesteps and  $V$  features,  $x \in \mathbb{R}^{T \times V}$  is tokenized via a convolution-subsampling module. The convolution-subsampling tokenizer comprises of two 1-D convolution layers with a kernel size of 3 and stride of 2 (Song et al., 2023). The resulting sequence of token has dimension  $N \times V$ , reducing the sequence length by 1/4, i.e.,  $N = T/4$ . These tokens are projected onto the input embedding  $\mathbf{X} \in \mathbb{R}^{N \times d}$  by an input projection layer. By adding [SOS] and [EOS] tokens, the sequence dimension becomes  $(N + 2) \times d$ . Given the  $L$  bidirectional generative layers, BiTimelyGPT alternates between forward and backward retention layers to train bidirectional contextualized representations. Moreover, the retention mechanism provides an efficient chunk-wise forward pass that segments an input sequence into multiple chunks (Sun et al., 2023a). Given a chunk size of  $C$ , the  $N \times d$  input embedding is reshaped into a  $C \times N/C \times d$  tensor. The output projection layer takes the output embedding with the shape  $N \times d$  in the last two layers, which are used to predict the original sequence of tokens with the shape  $N \times V$  for Next-Previous-Token Prediction task.

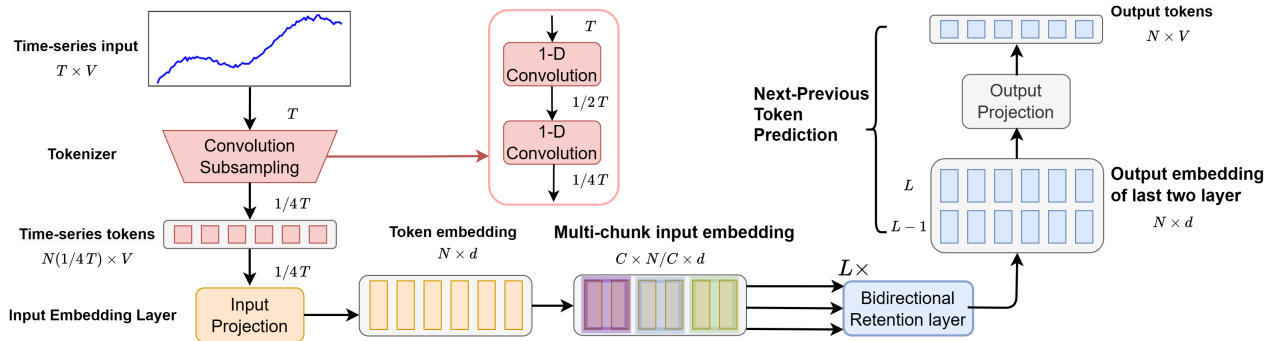


Figure 7. Schematic of the BiTimelyGPT Pre-Training Process

Table 6. The statistics of datasets. Note that the sequence length of the PPG-Dalia dataset varies across different dimensions.

Dataset	Task	Features	Timesteps	Sequences	Length	Classes
Sleep-EDF (Kemp et al., 2000)	Visualization	7	1.2B	400.7K	3,000	None
Sleep-EDF (sleep) (Kemp et al., 2000)	Classification	1	586.4M	195.5K	3,000	5
Epilepsy (Andrzejak et al., 2001)	Classification	1	2.0M	11.5K	178	2
PTB-XL (Alday et al., 2020)	Classification	12	109.2M	21,837	5,000	5
EMG (Goldberger et al., 2000)	Classification	1	306.0K	204	1,500	3
PPG-Dalia (Reiss et al., 2019a)	Regression	4	16.6M	64,697	256 & 512*	None
IEEPPG (Zhang et al., 2015)	Regression	5	3.1M	3,096	1,000	None
RR (Pimentel et al., 2017)	Regression	2	31.5M	7,870	4,000	None
HR (Pimentel et al., 2017)	Regression	2	31.8M	7,949	4,000	None
SpO2 (Pimentel et al., 2017)	Regression	2	31.8M	7,949	4,000	None

## B. Additional Information for Experiments

### B.1. Dataset Description

**Sleep-EDF dataset for Visualization.** Sleep-EDF dataset proposed by (Kemp et al., 2000) from PhysioBank (Goldberger et al., 2000) contains sleep cassette data obtained from 153 subjects. The collected whole-night polysomnographic (PSG) sleep recordings encompass 7 features: Electroencephalogram (EEG) (from Fpz-Cz and Pz-Oz electrode locations), electrooculogram (EOG) (horizontal), submental chin electromyogram (EMG), and an event marker. EEG and EOG signals were sampled at 100 Hz, while the EMG and event marker were sampled at 1 Hz. The sleep patterns correspond to the PSGs consist of five sleep stages: Wake (W), Non-rapid eye movement (N1, N2, N3) and Rapid Eye Movement (REM). This dataset contains a total of 1.2B timesteps, segmented into 400.7K sequences of 3,000 timesteps each. Its pre-training was utilized for visualization analyses detailed in Section 4.2, Section 4.3, and Section 4.4.

**Sleep-EDF (Sleep-stage only) dataset for Classification.** We leveraged only the sleep stage of the Sleep-EDF dataset for the classification task following existing studies (Eldele et al., 2021; Zhang et al., 2022a). In line with conventional practices, we selected the single EEG channel that captures signals from the Fpz-Cz electrode location. Since the Sleep-EDF dataset labels five sleep stages (i.e., W, REM, N1, N2 and N3), we only focused on EEG signals associated with these sleep stages, resulting in a total of 586.4 million timesteps. This dataset was segmented into 195.5K sequences, each with 3,000 timesteps.

**Epilepsy Seizure Classification.** Epileptic Seizure Recognition dataset (Andrzejak et al., 2001) comprises EEG measurements from 500 subjects. This dataset captures brain electrical activity from different regions and states, and are divided into segments of 23.6 seconds. The original dataset consists of five classes of EEG measuring eyes open, eyes closed, healthy brain region, tumor region, and seizure. The first four classes were merged into a single class as these classes are unrelated to epileptic seizure, enabling a binary classification of epileptic seizures. The dataset for classification consists of 2M timesteps, divided into 11.5K sequences, each containing 178 timesteps.

**PTB-XL Classification.** Physikalisch Technische Bundesanstalt large scale cardiology database (PTB-XL) (Alday et al., 2020) from PhysioBank (Goldberger et al., 2000) contains 21,837 clinical 12-lead ECG signals (male: 11,379 and female: 10,458) with a duration of 10 seconds each, sampled with a rate of 500 Hz. These signals are categorized based on a set of twelve leads (I, II, III, AVL, AVR, AVF, V1, V2, V3, V4, V5, V6), where the reference electrodes on the right arm are provided for each signal, resulting in twelve labels for classification. This dataset for classification comprises 21,837 samples, each spanning 5,000 timesteps, amounting to a total of 109.2M timesteps.

**EMG Classification.** EMG dataset from PhysioBank (Goldberger et al., 2000) captures the electrical activity resulting from neural stimulation of muscles. This dataset provides insights about muscle functionality and the corresponding nerves responsible for their control. This dataset contains single-channel EMG signals sampled with a rate of 4 KHz. EMG recordings were obtained from the tibialis anterior muscle of volunteers exhibiting different degrees of muscular and neural disorders, resulting in three classification labels. This dataset for classification comprises 306.0K timesteps, segmented into 204 sequences, each consisting of 1,500 timesteps.

**PPG-Dalia Regression.** PPG-Dalia dataset (Reiss et al., 2019a) is available from Monash University, UEA&UCR Time Series Regression Archive (Tan et al., 2021). This dataset captures photoplethysmograph (PPG) data for motion compensation and heart rate estimation. Data was collected from 15 subjects engaging in daily life activities using both wrist-worn (Empatica E4) and chest-worn (RespiBAN Professional) devices. All signals were sampled at 700 Hz. The ECG recording serve as a ground truth for heart rate. The PPG and 3D-accelerometer data are used to estimate heart rate, while accounting for motion artefacts. This dataset with a total of 16.6M timesteps was divided into 64,697 sequences, with varied lengths of 256 or 512 timesteps in different dimensions. The pre-training on this PPG-Dalia as well as the PTB-XL dataset was utilized for fine-tuning regression tasks.

**IEEEPPG Regression.** IEEEPPG dataset (Zhang et al., 2015) is sourced from Monash University, UEA&UCR Time Series Regression Archive (Tan et al., 2021). This dataset aims to estimate heart rate by utilizing PPG and ECG signals. The dataset includes two-channel PPG signals, three-axis acceleration signals, and one-channel ECG signals. These signals were recorded simultaneously and sampled at a rate of 125 Hz. This dataset for regression contains 3.1M timesteps, segmented into 3.096K sequences of 1,000 timesteps each.

**RR, HR and SpO2 Regression.** BIDMC Respiratory Rate (RR), heart rate (HR) and blood oxygen saturation level (SpO2) datasets (Pimentel et al., 2017) are available at Monash University, UEA&UCR Time Series Regression Archive (Tan et al., 2021). These datasets were obtained from the Physionet’s BIDMC PPG and Respiration dataset (Goldberger et al., 2000). They contain PPG and ECG signals sampled at a rate of 125 Hz, which are designed for estimating RR, HR, and SpO2. The three datasets for regression were segmented into sequences of 4,000 timesteps each, yielding: (1) 7,870 sequences in the RR dataset, totaling 31.5M timesteps; (2) 7,949 sequences in the HR dataset, encompassing 31.8M timesteps; (1) 7,949 sequences in the SpO2 dataset, also amounting to 31.8M timesteps.

## B.2. Experiment Details for BiTimelyGPT and Baselines

Given the demonstrated scaling law in the time-series datasets (Song et al., 2023), we tailored the hyperparameters and model parameters corresponding to the size of pre-training datasets: (1) 18 million model parameters for the SleepEDF dataset; (2) 7.5 million model parameters for the PTB-XL dataset; (3) 7.5 million model parameters for the regression for the PTB-XL and PPGDalia datasets. For a fair comparison, we set the same model parameters as well as architectures for BiTimelyGPT, transformer baselines, and recurrent models, as shown in Table 7.

Table 7. Configurations of BiTimelyGPT , transformer baselines, and recurrent models across different experiments and datasets

Pre-training Datasets	Sleep-EDF	PTB-XL	PTB-XL & PPGDalia
Downstream Task	Classification	Classification	Regression
Data Size (Timesteps)	1.2B	109.2M	109.2M & 16.6M
Model Parameters	18M	7.5M	7.5M
<b>BiTimelyGPT</b>			
Decoder Layers	12	8	8
Heads	8	8	8
Hidden Dim ( $Q, K, V, FF$ )	320,320,640,640	240,240,480,480	240,240,480,480
<b>Transformer Baselines including Encoder-decoder, Encoder-only, and Decoder-only</b>			
Enc-Dec Layers	6 & 6	4 & 4	4 & 4
Encoder Layers	12	8	8
Decoder Layers	12	8	8
Heads	8	8	8
Hidden Dim ( $Q, K, V, FF$ )	384,384,384,1536	288,288,288,1152	288,288,288,1152
<b>Recurrent Models</b>			
Layers	12	8	8
Hidden Dim	384	288	288